Research Report on Resonant Tunneling Effect in Double-Barrier Structures

Chengrui Tang[ID][a]

Institute for Advanced Study, Shenzhen University, Shenzhen, 518060, China

Keywords: Resonant Tunneling Effect, Double-Barrier, TMM.

Abstract: This study systematically investigates the resonant tunneling effect and transmission characteristics of double-barrier structures through theoretical analysis and numerical simulations. Based on the Schrödinger equation under the effective mass approximation, analytical expressions for the transmission coefficient and resonance conditions are derived, revealing that resonance energy levels are dominated by quantum well coupling effects. The transmission spectrum is proven to exhibit a Lorentzian-shaped distribution near resonance energies. Further numerical calculations using the transfer matrix method (TMM) validate the conservation of probability ($T + R \approx 1$) and demonstrate a single dominant resonance peak ($T > 0.9$). The results indicate that barrier height (V_0), barrier width (w), and well width (d) significantly influence the position and width of resonance peaks, providing a theoretical foundation for optimizing resonant tunneling devices. By combining analytical derivations with numerical verification, this work deepens the understanding of electron transport mechanisms in multi-barrier quantum structures, offering potential applications in high-speed electronic devices and quantum engineering.

1   INTRODUCTION

Quantum tunneling is a hallmark phenomenon of quantum mechanics. It distinguishes quantum mechanics from classical physics by enabling microscopic particles to traverse potential barriers that exceed their energy. This effect is not only a fundamental prediction of quantum theory (such as Gamow's theory of alpha decay) but also the core physical principle behind modern nanoelectronic devices. From the atomic-scale resolution of scanning tunneling microscopes to the terahertz (THz) rectification in triple-barrier resonant tunneling diodes with on-chip antennas, quantum tunneling has continuously redefined the frontiers of device physics (Arzi et al., 2019).

The phenomenon of quantum tunneling, where particles traverse classically forbidden energy barriers via wavefunction penetration, serves as the foundational mechanism driving the functionality of engineered multi-barrier heterostructures. Recent advancements in multi-barrier heterostructures reveal a rich interplay between quantum confinement and transport dynamics. For instance, asymmetric barrier–well–barrier structures employing ferroelectric HfO_2 layers demonstrate a 200% enhancement in tunneling electroresistance (TER) under electric field modulation, providing a non-volatile memory mechanism that outperforms traditional memristive devices (Chang and Xie, 2023). Concurrently, resonant tunneling in ZnO/In_2O_3 heterojunctions has enabled room-temperature NO_2 gas detection with sub-ppm sensitivity, where quantum well coupling dynamically regulates charge carrier mobility through selective barrier penetration—a paradigm shift in solid-state sensing (Liang et al., 2021). In terms of resonant tunneling diodes, a terahertz coherent receiver using a single resonant tunnelling diode and optimum device parameters to attain the highest peak-to-valley current ratio (PVCR) in resonant tunneling diodes was proposed (Nishida et al., 2019; Ipsita, Mahapatra, Panchadhyayee, 2021).

The exploration of tunneling mechanisms now extends beyond conventional semiconductors. In metallic multi-quantum-well systems, resonant

inelastic tunneling spectroscopy has uncovered an energy-selective hot carrier injection pathway, enabling precise control over plasmonic energy conversion efficiencies by exploiting subband coupling in stacked metal-insulator interfaces (Zhang et al., 2023). Meanwhile, pseudospin-1 Dirac–Weyl fermion systems exhibit spin-momentum-locked resonant tunneling channels, where quantized conductance plateaus emerge from the interplay between chiral pseudospin textures and double-barrier potentials—a phenomenon that challenges classical scattering theory and opens avenues for topological quantum devices (Zhu, 2024).

The resonant tunneling effect is a significant phenomenon in quantum mechanics, particularly in semiconductor heterostructure devices such as resonant tunneling diodes. As the simplest multi-barrier system, the study of resonant tunneling in double-barrier structures lays the foundation for understanding more complex multi-barrier systems (Xu et al., 1991). This study combines numerical simulations and theoretical analysis to investigate the transmission coefficient, resonance conditions, and spectral features of double-barrier structures, elucidating their physical principles and device potential.

2 THEORETICAL MODEL

2.1 Derivation

Consider a double-barrier structure composed of two barriers with height V_0 and thickness L_b, and a well with width L_w. The electron energy E satisfies $0 < E < V_0$, with electrons incident from the left and tunneling through the barriers to the right. The wavefunction in each region obeys the effective mass Schrödinger equation:

$$-\frac{\hbar^2}{2m^*}\frac{d^2\psi}{dx^2} + V(x)\psi = E\psi, \qquad (1)$$

where m^* is the effective mass, $\hbar$ is the reduced Planck's constant, ψ is the electron wave function. The potential distribution is:

$$V(x) = \begin{cases} 0 & \text{(incident region),} \\ V_0 & \text{(barrier regions),} \\ 0 & \text{(well region),} \\ V_0 & \text{(right barrier region).} \end{cases} \qquad (2)$$

The continuity of the wavefunction and its first derivative at the boundaries is solved using the transfer matrix method. The transmission coefficient T is derived as (Tsu, 1973; Kane, 1969):

$$T = [1 + (AH)^2]^{-1}, \qquad (3)$$

where:

$$A = \frac{k_A^2 + k_B^2}{2k_A k_B} \sinh(k_B L_b), \qquad (4)$$

$$H = 2\cosh(k_B L_b)\cos(k_A L_w) -$$
$$\frac{k_A^2 - k_B^2}{2k_A k_B}\sinh(k_B L_b)\sin(k_A L_w), \qquad (5)$$

with $k_A = \sqrt{2m^*E}/\hbar$ and $k_B = \sqrt{2m^*(V_0 - E)}/\hbar$.

When $H = 0$, the transmission coefficient $T = 1$, indicating complete resonant tunneling. The resonance energy E_0 approximates the quantized energy level of the well, demonstrating that resonance levels are determined by the bound states of the well. At this condition, the electron wavefunction forms a standing wave in the well, maximizing tunneling probability.

Near the resonance energy E_0, the transmission coefficient follows a Lorentzian distribution:

$$T \approx \left[1 + \left(\frac{E - E_0}{\Delta E}\right)^2\right]^{-1}, \qquad (6)$$

where the full width at half maximum (FWHM) $\Delta E = \left[A(E_0)\frac{dH}{dE}\big|_{E=E_0}\right]^{-1}$ reflects the sharpness of the resonance. A smaller ΔE corresponds to a longer resonance lifetime.

2.2 Physical Implications

In terms of quantum well coupling, the finite barrier height couples the quantized energy levels of the well to the external environment, causing resonance energies to deviate slightly from the eigenvalues of an isolated well. For applications, the high selectivity of Lorentzian-shaped transmission spectra is valuable for high-speed electronic devices (e.g., terahertz oscillators) and quantum computing.

3 NUMERICAL METHODS

A double-barrier structure is defined by two barriers ($V_0 = 0.3$ eV, $w = 2$ nm) and a well ($d = 5$ nm). Electrons with energy $0 < E < V_0$ tunnel through the barriers, governed by the effective mass Schrödinger equation.

The transfer matrix method (TMM) is employed to compute transmission (T) and reflection (R) coefficients:

First calculate wavevector and determine k_i (real for propagating waves, imaginary for evanescent waves) based on E and V_0.

$$k_j = \begin{cases} \sqrt{2m^*(E - V_j)}/\hbar & (E > V_j) \\ i\sqrt{2m^*(V_j - E)}/\hbar & (E < V_j) \end{cases} \qquad (7)$$

where $j = 1,2,3,4,5$ corresponds to the five regions (left incident region, left barrier, well, right barrier, right exit region). Evanescent waves ($\text{Im}(k) \neq 0$) dominate in barrier regions when $E < V_0$. Then, construct interface matrices enforcing wavefunction continuity at boundaries. For each interface between regions j and $j + 1$, the interface matrix is derived from boundary conditions:

$$M_{j \rightarrow j+1} = \begin{bmatrix} 1 & 1 \\ k_{j+1} & -k_{j+1} \end{bmatrix}^{-1} \begin{bmatrix} 1 & 1 \\ k_j & -k_j \end{bmatrix} \quad (8)$$

And propagation Matrices account for model phase accumulation in barriers and wells. Propagation matrices incorporate phase evolution across each region:

$$M_{\text{propagate},j} = \begin{bmatrix} e^{ik_j L_j} & 0 \\ 0 & e^{-ik_j L_j} \end{bmatrix} \quad (9)$$

Finally, multiply matrices sequentially to derive $T = |t|^2$ and $R = |r|^2$ and validate $T + R = 1$ to complete the conservation check.

4 RESULTS AND DISCUSSIONS

Figure 1 shows T and R versus energy, meaning when the electron energy approaches the quantized energy level of the potential well, $T \approx 1$ and $R \approx 0$, indicating perfect resonant tunneling and the appearance of resonant peaks. The transmission peak near E_0 matches theoretical predictions, with FWHM ΔE dependent on barrier parameters.
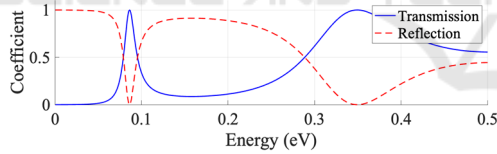
Figure 1: Quantum Tunneling in Double Barrier Structure: $V_0 = 0.3 \text{ eV}, w = 2 \text{ nm}, d = 5 \text{ nm}$(Picture credit: Original).

Figure 2 shows with the increase of the barrier height V₀, the formant moves towards the high energy direction and the peak width Narrows. This is because the higher barrier enhances the quantization effect of the quantum well, making the electrons more tightly bound in the potential well, resulting in higher resonance energy and narrower formant.
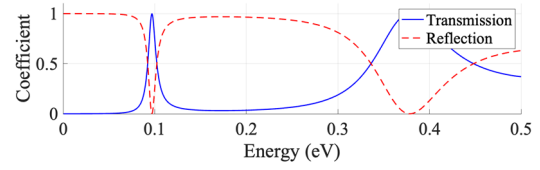
Figure 2: $V_0 = 0.4 \text{ eV}, w = 2 \text{ nm}, d = 5 \text{ nm}$(Picture credit: Original)

Figure 3 shows an increase in the barrier width enhances the quantum confinement effect, bringing the resonance energy closer to the eigenvalue of the isolated potential well. This is because the wider barrier limits the movement of electrons in the lateral direction, resulting in a more pronounced split of the quantized energy levels, thus bringing the resonance energy closer to the eigenvalue of the isolated potential well.
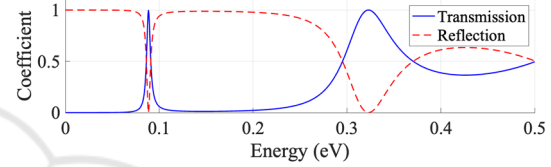
Figure 3: $V_0 = 0.3 \text{ eV}, w = 3 \text{ nm}, d = 5 \text{ nm}$(Picture credit: Original)

Figure 4 shows that the increase of the potential well width will reduce the quantized energy level spacing, which may lead to the appearance of the multi-peak structure. This is because a wider potential well provides more room for electrons to move, making the distribution of quantized energy levels more dense, resulting in multiple formants in the transmission spectrum.
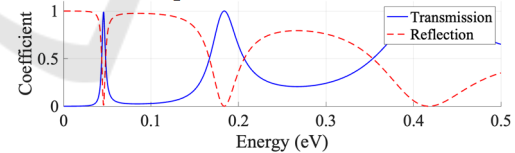
Figure 4: $V_0 = 0.3 \text{ eV}$，$w = 2 \text{ nm}, d = 8 \text{ nm}$(Picture credit: Original)

Figure 5 confirms $T + R = 1$ in above cases, ensuring numerical consistency and wavefunction integrity. The verification of probability conservation is an important part of numerical simulation, which not only ensures the physical rationality of the calculated results, but also provides a reliable numerical reference for the subsequent experimental research and device design, and enhances the reliability of the research results.
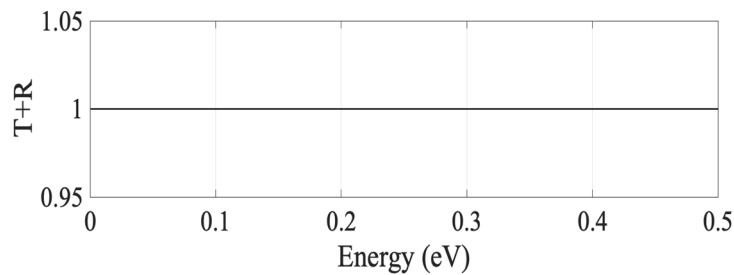
Figure 5: Probability Conservation (Picture credit: Original)

5 CONCLUSION

In conclusion, the research analyzes the transmission coefficient, resonance conditions, and spectral features of double-barrier structures, elucidating their physical principles. The resonance condition for double-barrier structures is determined by $H = 0$, with resonance energies approximating the quantized levels of the well. The transmission spectrum near resonance energies exhibits a Lorentzian profile, with FWHM strongly dependent on barrier parameters. Numerical simulations validate resonant tunneling in double-barrier structures, with Lorentzian transmission spectra aligning with theory. The TMM accurately computes T and R while preserving probability conservation. Resonance characteristics are tunable via barrier/well parameters, enabling tailored device design and the performance of the device can be optimized. This provides a broad prospect for the development of new high-speed electronic devices and quantum engineering applications. However, one limitation about the research is that the current model assumes elastic tunneling and ideal rectangular barriers, neglecting inelastic scattering effects (e.g., electron-phonon coupling) and interface roughness, which may lead to deviations in high-bias or high-temperature regimes. Incorporating non-equilibrium Green's function (NEGF) or time-dependent density functional theory (TDDFT) to account for inelastic scattering and defect-mediated tunneling, enhancing predictive accuracy under non-ideal conditions is necessary for future improvement work.

REFERENCES

Arzi, K., Clochiatti, S., Suzuki, S., Rennings, A., Erni, D., Weimann, N., Asada, M., Prost, W., 2019. Triple-barrier resonant-tunnelling diode THz detectors with on-chip antenna. In 2019 12th German Microwave Conference (GeMiC), Stuttgart, Germany, pp. 17–19.

Chang, P., Xie, Y., 2023. Ferroelectric tunnel junction based on asymmetric barrier–well–barrier structure: the role of resonant tunneling. *IEEE Transactions on Electron Devices*, 70(5), 2282–2290.

Ipsita, S., Mahapatra, P.K., Panchadhyayee, P., 2021. Optimum device parameters to attain the highest peak to valley current ratio (PVCR) in resonant tunneling diodes (RTD). *Physica B: Condensed Matter*, 611, 412788.

Kane, O.E., 1969. *Tunneling Phenomena in Solids*. Plenum Press.

Liang, X., Zhang, J., Du, L., Zhang, M., 2021. Effect of resonant tunneling modulation on ZnO/In_2O_3 heterojunction nanocomposite in efficient detection of NO_2 gas at room temperature. *Sensors and Actuators B: Chemical*, 329, 129230.

Nishida, Y., Nishigami, N., Diebold, S., Kim, J., Fujita, M., Nagatsuma, T., 2019. Terahertz coherent receiver using a single resonant tunnelling diode. *Scientific Reports*, 9, 18125.

Tsu, R., Esaki, L., 1973. Tunneling in a finite superlattice. *Applied Physics Letters*, 22(11), 562–564.

Xu, H., Wang, Y., Zhang, F., Chen, G., 1991. Resonant tunneling condition in ABCBA–type rectangular double–barrier structures. *Physica Status Solidi B: Basic Solid State Physics*, 163.

Zhang, Y., Lepage, D., Feng, Y., Zhao, S., Chen, H., Qian, H., 2023. Resonant inelastic tunneling using multiple metallic quantum wells. *Nanophotonics*, 12(16), 3313–3321.

Zhu, R., 2024. Transport properties of the resonant tunneling structures based on the pseudospin-1 Dirac–Weyl fermions. *Physica B: Condensed Matter*, 687, 416091.